International Journal of Impact Engineering 62 (2013) 114–128

Contents lists available at SciVerse ScienceDirect

International Journal of Impact Engineering

journal homepage: www.elsevier.com/locate/ijimpeng

Impact response of aluminum corrugated core sandwich panels

H.N.G. Wadley*, K.P. Dharmasena, M.R. O'Masta, J.J. Wetzel

Department of Materials Science and Engineering, University of Virginia, Charlottesville, VA 22904-4745, USA

ARTICLE INFO

Article history:
Received 28 January 2013
Received in revised form
22 April 2013
Accepted 9 June 2013
Available online 27 June 2013

Keywords:
Ballistics
Sandwich panels
Aluminum alloys
Alumina

ABSTRACT

The mechanisms of projectile penetration of extruded 6061T6 aluminum alloy sandwich panels with empty and alumina filled, triangular corrugated cores have been experimentally investigated using zero obliquity, 12.7 mm diameter hard steel projectiles whose diameter was about a half that of the core's unit cell width. We find that low momentum impacts are laterally deflected by interactions with the inclined webs of the empty core. Complete penetration occurred by shear-off within the impacted front face sheet, followed by stretching, bending and tensile fracture of the core webs and finally shear-off within the back face sheet. This combination of mechanisms was less effective at dissipating the projectiles kinetic energy than the shear-off (plugging) mechanism of penetration of the equivalent solid aluminum panel. Inserting ballistic grade alumina prisms in the triangular cross section spaces of the corrugated core significantly increased the panel's ballistic resistance compared to the empty panel. The presence of the hard ceramic led to severe plastic deformation and fragmentation of the projectile and comminution and macroscopic fracture of the ceramic. The Al/Al_2O_3 hybrid panel ballistic limit was reached when pairs of parallel cracks formed in the rear face sheet at core web-face sheet nodes. The separation distance between these cracks was dependent upon the location of the impact with respect to that of the web-face sheet nodes. Nodal impacts resulted in pairs of fractures that were separated by one cell width and a critical velocity below that of the equivalent solid plate. Impacts mid-way between pairs of nodes resulted in back face sheet crack pairs separated by twice the cell width, and a critical velocity higher than the equivalent solid plate. Using X-ray tomography we show this resulted from the formation of oval (not circular) cross section fracture conoids in the ceramics. The conoid angle was about 60° in the extrusion direction but only 30° in the transverse direction. This observation may have interesting consequences for a panel's resistance to a second, close proximity impact.

1. Introduction

It is an inconvenient fact that materials with the highest specific[1] resistance to single impacts near their ballistic limit, perform poorly when subjected to a second nearby impact. Conversely, materials that have the best multi-hit response do not have the highest single impact ballistic resistance [1]. Fig. 1 schematically illustrates the influence of material properties upon the penetration process in metals, composites and ceramics. A second impact whose fracture conoid intersects that of the first experiences reduced penetration resistance. The reduction in the radial extent of damage in some composites and most ductile metals then provides superior multi-hit response, but at reduced ballistic limit compared with a ceramic.

This observation has stimulated the development of multilayered and composite material systems that possess a balance of ballistic properties that are better matched to applications. It has also led to interest in segmented systems in which a high (single hit) ballistic resistant material, such as a square [2] or hexagonal [3] shaped ceramic tile, is embedded in a tougher material such as a metal alloy or polymer. Since it is beneficial to allocate a fraction of the panels mass to a back support and cover plate (to confine the ceramic), these hybrid structures often take the form of sandwich panels in which the cores consist of periodic cellular structures filled with ceramic.

Metallic sandwich panels with unfilled cellular cores can exhibit superior bending stiffness and strength compared to solid (monolithic) plates of the same alloy and mass per unit area (areal density) [4]. When applied to ballistic applications they offer potentially useful multifunctionality. Many unfilled core topologies have been

* Corresponding author.
E-mail address: haydn@virginia.edu (H.N.G. Wadley).
[1] Ballistic resistance divided by target density and thickness.

0734-743X
http://dx.doi.org/10.1016/j.ijimpeng.2013.06.005

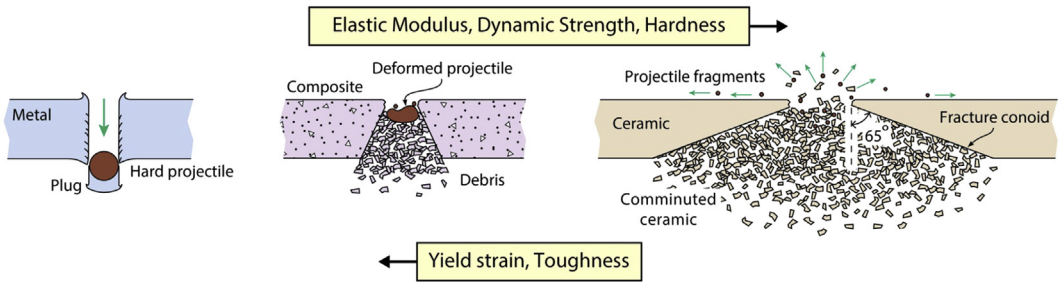

Fig. 1. The effects of material properties on projectile penetration near the ballistic limit of light targets.

explored for structural load support applications including those based upon honeycombs [5], prismatic corrugations [6] and truss structures (including some with hollow trusses) [7,8]. When the panel mass is optimally distributed between the front face, core and back face sheet, the high bending resistance of sandwich panels can reduce the back face deflection suffered by impulsively loaded, edge supported panels [9–11]. This benefit is enhanced if fluid structure interaction effects can be exploited to minimize impulse reflection [12], and inertial strengthening (stabilization) and/or rate dependent material hardening increases the cores strength under dynamic loading [13,14]. Small (of order 10%) reductions in impulse can occur when sandwich structures are impulsively loaded by high velocity sand [15] or air [16], but much larger reductions have been reported for water [17] propagated shocks. In all cases, the higher bending resistance of sandwich structures can further reduce back side deflections compared to equivalent solid plates. The bi-functionality of efficient stress support and impulse mitigation has led to considerable interest in low density (light) metal variants for structures that could be loaded by nearby explosive events. Since projectiles often accompany such events, there is additional interest in the ballistic response of metallic sandwich panel structures.

Relatively little is known about the resistance of light metal sandwich panels to localized projectile impact. A recent study of the impact of stainless steel sandwich panels with low volume fraction (2.6%) pyramidal lattice cores by low strength (plain carbon) steel spheres found that the empty sandwich panel's ballistic limit was experimentally indistinguishable from that of a solid stainless plate of identical mass per unit area, even though the mechanisms of projectile penetration were significantly different [18]. The experimental study also indicated that on a unit mass basis, identical structures made from a 6061T6 aluminum alloy performed better than the stainless steel. The projectile used in these investigations was of similar strength to the sandwich panel materials, and since significant projectile deformation (and impact energy dissipation) occurred within the projectile, the intrinsic behavior of the panel was difficult to ascertain. These low strength cores also have insufficient crush strength for practical blast mitigation applications. Furthermore, the slender (low volume fraction) trusses provided little resistance to penetration by a projectile and the small area of the (braze bonded) nodes between the trusses and the faces led to early node failure during projectile impact.

Recently, a novel extrusion-based method has been developed to fabricate sandwich panels from a 6061T6 aluminum alloy. Panels with a triangular corrugated core structure that occupied 25% of the volume between the faces were extruded [15], and had a compressive core strength of 60 MPa and node failure strength the same as the faces. When loaded by explosively accelerated wet sand, the back face sheet deflections of these panels were significantly less than those of solid plates of the same alloy and areal density. The thicker inclined webs of this core offer interesting possibilities for potentially deflecting projectiles, and the large empty regions between the webs provide opportunities to incorporate ballistic resistant materials into a hybrid core.

Here we begin an exploration of the mechanisms of projectile penetration in this model aluminum corrugated core sandwich panel system. We use very hard steel spherical projectiles whose diameter was about a half that of the core cell width, and investigate the effect of inclined webs upon the penetration process in scenarios where the projectile does not suffer significant plastic deformation or fracture. We impact the panels at zero obliquity at either a node (an apex of the triangular prism void) or mid-way between nodes (at a prism base) and focus upon the mechanisms of panel response compared to those of an equivalent[2] solid plate. We then insert ballistic grade alumina prisms into the open triangular cross section cells of the sandwich panel, and investigated their effect upon the mechanisms of projectile interaction. The ceramic inserts are shown to cause significant plastic deformation and fracture of the projectile leading to an increase in the ballistic limit compared to the empty panel. However, the ballistic limit of the ceramic filled panels is found to be highly dependent on the relative location of the impact within a unit cell of the core; impacts on the base of a prism are more effectively resisted than those on an apex. The webs are found to reduce the fracture conoid angle on the plane transverse to the extrusion direction creating an oval shaped conoid with implications for resistance to a second nearby impact. The inclined surfaces of the webs/ceramics also appear to alter the trajectory of the debris that exits the rear of a defeated panel.

2. Sample fabrication

2.1. Sandwich panel

Approximately 3 m long, corrugated core, 6061 aluminum sandwich panels were fabricated from 17.8 cm diameter billets using a 300 ton, direct porthole extrusion process. The extruded panels were solutionized, water quenched and heat treated to a T6 condition. Vertical webs at the sides of the extrusions were removed, and the resulting 135.9 mm wide by 133.4 mm long test structure geometry is shown in Fig. 2(a). The core consisted of triangular cross section prismatic voids with the apex of the prisms alternating between the top and bottom of the panel. The structures unit cell is shown in Fig. 2(b). The width of the triangular void base was 22 mm and its height was 19.3 mm. The prismatic voids were separated by webs with a thickness of 3.2 mm and an inclination angle of 60°. The core was integrally bonded to 5.2 mm thick face sheets. The relative density (volume fraction of metal in a unit cell) of the corrugated core, $\bar{\rho}$ was 25%, and the mass per unit area of the panels, $\rho_a = (2h + c\bar{\rho}\rho) = 41.6 \pm 0.1$ kg m^{-2} where h is the face sheet thickness, c is the thickness of the core, and ρ is the density of the

[2] Identical alloy and similar density-thickness (aerial density) product.

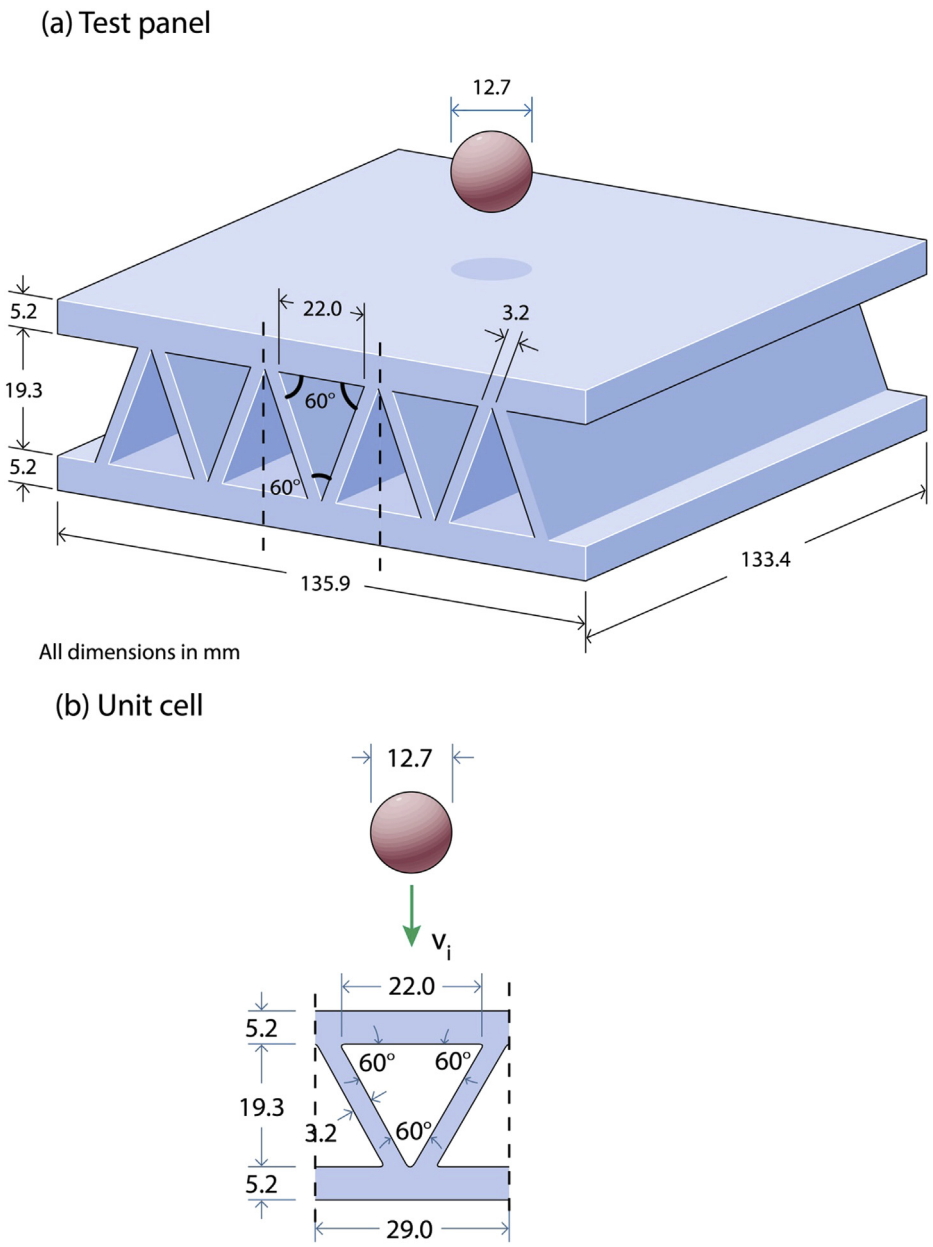

Fig. 2. (a) The triangular corrugated core sandwich panel with edges removed. The core relative density was 25%, and the panel's mass per unit area was 41.6 ± 0.1 kg m^{-2}. (b) A unit cell of the sandwich panel and projectile.

aluminum alloy. The panel's mass fractions distributed between impact face, the core and rear face were 0.34:0.32:0.34.

The uniaxial stress verses strain response of the parent 6061T6 aluminum alloy was measured in the extrusion direction using tensile test coupons extracted from the extrusions. The Young's modulus was 72 GPa, the yield strength was 290 MPa, the ultimate tensile strength was 329 MPa and the engineering strain to fracture was 8.9%.

2.2. Aluminum–alumina composite core

Grade AD-995 alumina tiles were obtained from CoorsTek (Golden, CO) with dimensions 15.2 cm × 12.7 cm × 2.5 cm, Fig. 3 (a). This ceramic has a hardness of 14.1 GPa, a compressive strength of 2.6 GPa, a Young's modulus of 370 GPa, a density of 3.9×10^3 kg m^{-3}, a fracture toughness of 4–5 MN m$^{-3/2}$ and a grain size of 6 μm. The alumina tiles were diamond blade saw cut into triangular prisms that were a "sliding" fit to the inside of the corrugated core channels, Fig. 3(b). A Lord (Cary, NC) grade 305 general purpose, medium viscosity, two-component epoxy adhesive was used to bond the ceramic to the interior metal walls of the corrugated aluminum structure as shown in Fig. 3(c). The mass per unit area of the hybrid core structure was 97 kg m^{-2}.

2.3. Solid aluminum plates

Solid plates of 6061T6 aluminum with thicknesses of 15.9 and 36.6 mm were machined to create test structures with the same lateral dimensions as the ballistic test structures described above. The thinner plate's areal density was 42.9 kg m^{-2} and matched that

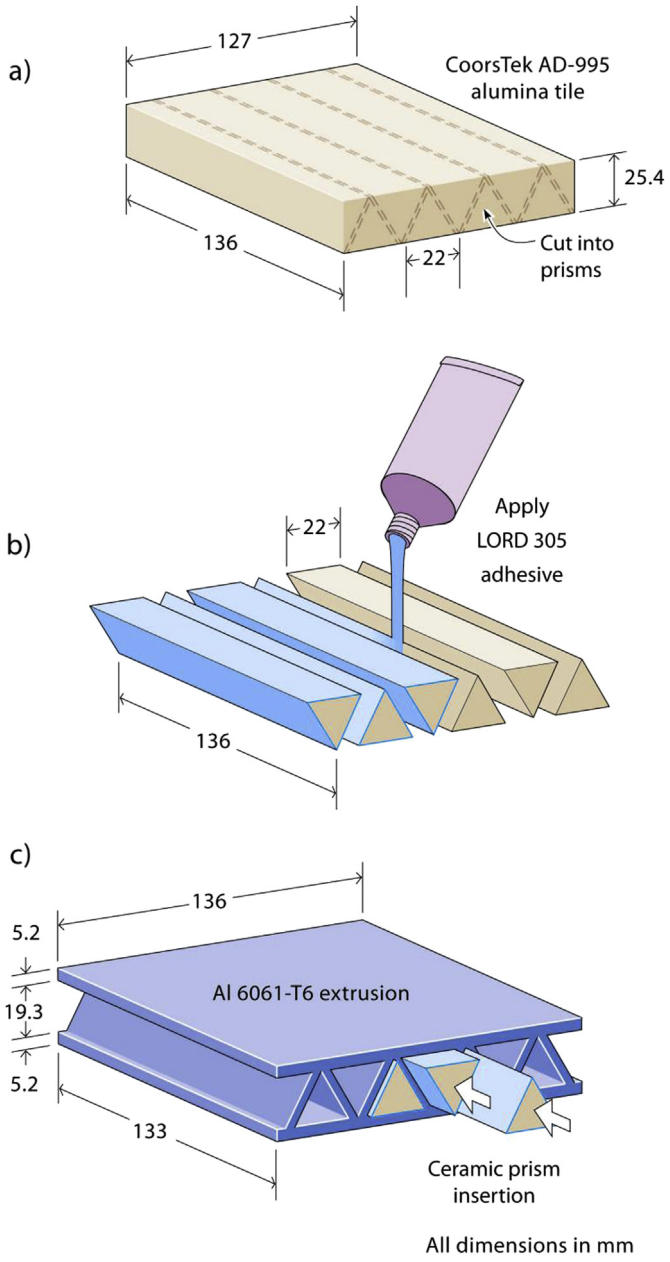

Fig. 3. Ceramic prism integration in hybrid core sandwich panels. (a) 136 mm × 127 mm × 25.4 mm thick, Coorstek grade AD-995 alumina tile showing prism cuts. (b) Application of adhesive to 136 mm × 22 mm × 19.3 mm ceramic prisms. (c) Insertion of prisms into the open spaces of the corrugated core sandwich panel. The filled panel's areal density was 97 kg m^{-2}.

of the empty sandwich panels. The thicker plates had a mass per unit area of 98.9 kg m^{-2}; similar to that of the hybrid core samples filled with alumina.

3. Ballistics test procedure

Ballistic testing was conducted with 12.7 mm diameter hardened 52100 chrome steel spheres with a composition of 1.45% Cr, 0.3% Mn, and 0.25% Si. They had a measured compressive yield strength of 2.4 GPa, a failure strength of 3.2 GPa and a Young's modulus of 200 GPa. The initial ballistic experiments were performed at H.P. White Laboratory, Inc. (Street, MD), Chesapeake Testing (Belcamp, MD). Subsequent experiments utilized the

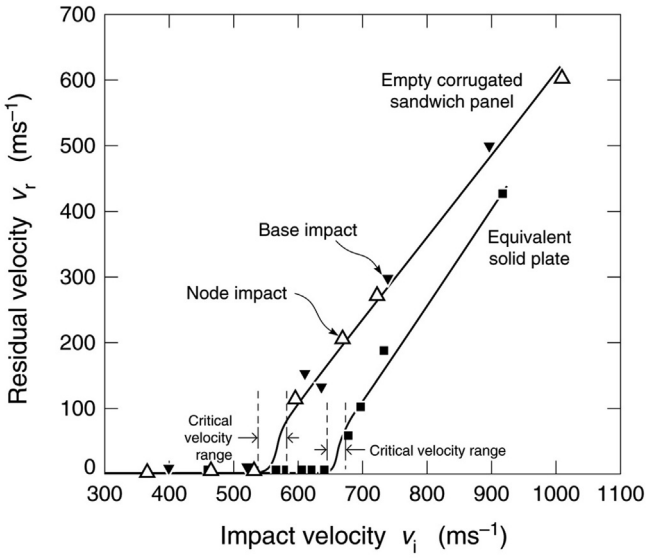

Fig. 4. The residual (exit) projectile velocity plotted against impact velocity for the empty corrugated core sandwich panel with an aerial density of 41.6 kg m^{-2} and a solid plate of the same aluminum alloy and similar mass/unit area (42.9 kg m^{-2}).

University of California at Santa Barbara light gas gun to launch sabot projectile-combinations at predetermined locations (apex or mid-span between nodes) on targets in a low vacuum test chamber. In these latter experiments only impacts within ±2.5 mm of the intended impact location were utilized in the study. High-speed camera systems and break screens were used to measure the impact and residual projectile velocities. Paper break screens recorded the impact velocity (V_i) to a precision of ±0.4, 1.7 and 3.7 m s^{-1} for projectile velocities of 500, 1000 and 1500 m s^{-1} respectively. Laser break screens and a high-speed camera were used to measure residual projectile velocity (V_r). The high-speed camera frame rate was 50,000 frames per second. Using these methods, the precision of the exit velocity component normal to the sample surface was ±1.0, 3.0 and 5.0 m s^{-1} for residual velocities of 100, 300 and 500 m s^{-1} respectively. Some of the tested structures were characterized by X-ray computed tomography (XCT) and then all were sectioned by water-jet cutting to reveal the mechanisms of projectile penetration.

4. Impact of corrugated core sandwich

4.1. Empty core response

The sandwich structures were impacted at either an apex of a corrugation (the node location) or mid-way between two nodes (a base impact location) and the residual velocity measured as a function the incident velocity. Fig. 4 shows the dependence of the empty sandwich panels residual velocity upon impact velocity for impact velocities of 360–1000 m s^{-1}, and compares this response with that of the equivalent solid plate. The critical impact velocity at which penetration of the sandwich panel occurred was between 530 and 590 m s^{-1} and was independent of impact location, while that of the solid plate was about 130 m s^{-1} higher (650–675 m^{-1}). The residual velocity of projectiles that perforated the sandwich panel was insensitive to the location of impact (node, or base impact location).

After testing, the sandwich panels and solid plates were cross sectioned to expose a plane centered on the impact location. Fig. 5 shows three examples of a node impact. In all cases, the steel

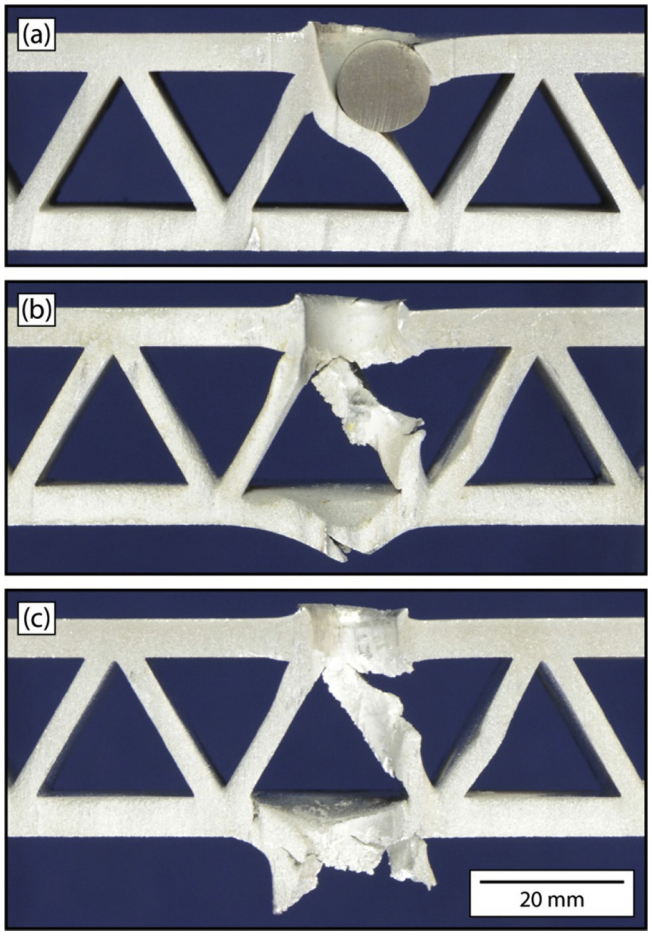

Fig. 5. Empty corrugated core sandwich panel impacted near a node by a 12.7 mm diameter steel projectile with impact velocities of (a) 368 m s^{-1}, (b) 453 m s^{-1} and (c) 676 m s^{-1}.

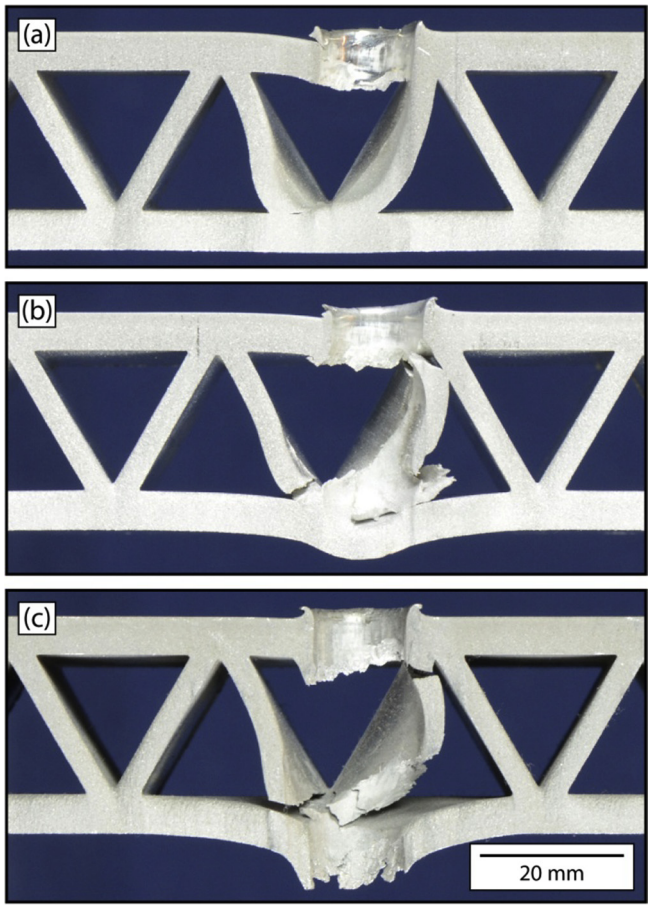

Fig. 6. The empty corrugated core sandwich panel after base impact by a 12.7 mm diameter steel projectile with an incident velocity of (a) 401 m s^{-1}, (b) 510 m s^{-1} and (c) 638 m s^{-1}.

projectile penetrated the front face sheet by shear plugging. At the lowest impact velocity of 368 m s^{-1} the projectile was arrested within the front face sheet, Fig. 5(a), with no detectable permanent deformation of the back face sheet. The projectile was arrested upon contact with a web, causing the web to bend inwards and away from the projectile. The lateral component of force required to do this caused a sideways motion of the projectile opposite in direction to that of web deflection. As the impact velocity was increased, Fig. 5(b), the inclined web was perforated by shear plugging, and the projectile (not shown) was arrested when contact was made with the rear face sheet. As the impact velocity was increased above the ballistic limit, Fig. 5(c), penetration of the back face sheet occurred by plugging.

Fig. 6 shows cross-sections of several sandwich panels impacted at base locations between pairs of nodes. Projectile penetration of the front face sheet again occurred by adiabatic shear (plugging). However, the projectiles then impacted V-shaped webs causing outward bending. Impact of the rear face caused tensile fracture of the web-face sheet attachments at the bottom of the "V", Fig. 6(b). These nodal fractures extended several centimeters in the extrusion direction. At higher velocities, Fig. 6(c), localized bending of the back face sheet occurred followed by shear plug penetration.

4.2. Solid aluminum plate impact

Cross-sectional views of the solid plate after impact at various velocities are shown in Fig. 7. The cross-sectional images are consistent with penetration by shear plugging with some crater formation involving lateral and reverse (upward) material flow at the front surface, and bending with some peripheral fracture at the exit hole. Fig. 8(a) shows a high-speed video image of the rear of a perforated target that confirms the plug mechanism of penetration. Both the plug and projectile (and a small panel fragment from the periphery of the exit region) can be seen exiting the sample 300 μs after impact. Fig. 8(b) shows the recovered plug and still undeformed projectile (with some aluminum alloy adhering to the hemisphere that had been in contact with the sample during penetration).

5. Ceramic filled sandwich panel

5.1. Hybrid panel behavior

Impact of the alumina filled sandwich panels resulted in an impact response mechanism that was dependent upon where the projectile impacted the structures unit cell; impacts at the center of the 22 mm wide ceramic prism base interacted very differently to those that impacted a prism apex. We therefore performed two series of experiments to examine these limiting impact scenarios and show the ballistic response for nodal and base impacts in Fig. 9(a). Impacts with the ceramic prism base had a critical velocity of approximately 1300 m s^{-1} whereas those with a prism apex more easily penetrated the structure, and the critical velocity was about 250 m s^{-1} less than that for the base. Above the ballistic limit,

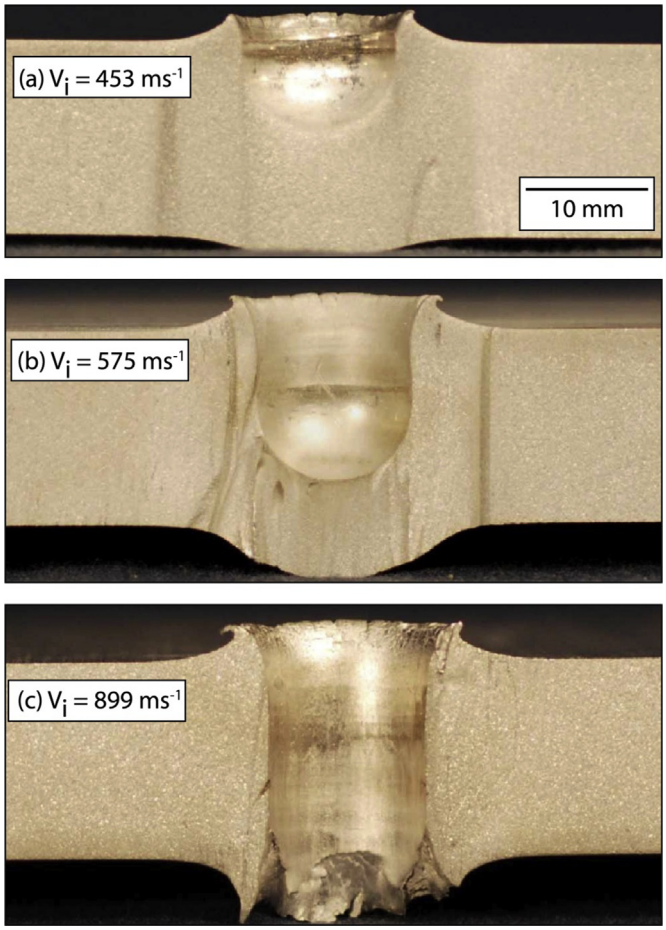

Fig. 7. The effect of increasing impact velocity on the penetration of 15.9 mm thick (aerial density of 42.9 kg m^{-2}) 6061T6 aluminum plates. (a) 453 m s^{-1}, (b) 575 m s^{-1} and (c) 899 m s^{-1}.

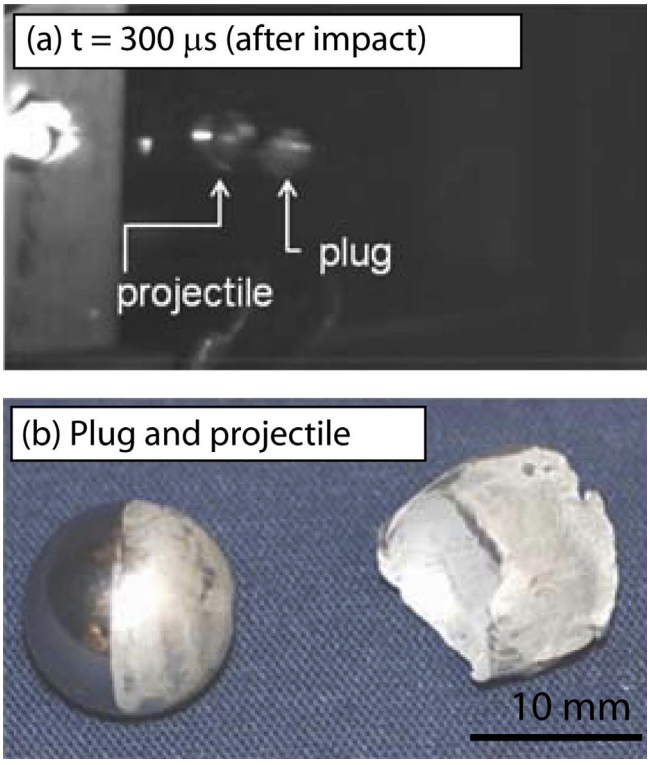

Fig. 8. (a) A high-speed video image of the projectile and plug following impact of the solid plate by a 12.7 mm diameter projectile at an impact velocity of 729 m s^{-1}. The bright white region to the left is the hole in the back face of the sample. (b) The projectile and a recovered plug from the same experiment.

the debris that exited the rear face of the sample was deflected by the hybrid core and exited at an angle between 45° and 80° to the surface of the sample. We were only able to measure the ejecta velocity component normal to the back surface of the sample, and the slope of this component of residual velocity versus impact velocity relation above the critical velocity was 0.83, and was the same for both impact locations. We then proceeded to examine the impact mechanisms at each impact location.

5.1.1. Base impacts

Fig. 10 shows a sequence of high-speed video images of the rear face of a sample impacted on a prism base by a projectile with an impact velocity of 1492 m s^{-1}. The corrugations within the sample were aligned vertically in this view of the sample. At 40 μs after impact, the rear of the target had suffered a significant (rectangular-shaped) out of plane deflection. The width of the deformed region was 56 mm and did not increase further with time. The vertical white linear coloration at the right side of the deformation corresponds to the initiation of a fracture that elongated in the panels extrusion direction. A similarly elongated region of large deformation can also be seen near the left side of the deformed region. As time progressed, this region began to fracture and the crack pair extended in the vertical direction. A third collinear crack mid-way between the outer pair also eventually developed. The vertical extent of the deformed face sheet increased with time to a length of about 85 mm. At about 160 μs after impact white debris began to be emitted from the crack on the left at a shallow angle to the back face surface normal. A horizontal crack in the aluminum face sheet also began to form and eventually linked the side and central vertical cracks allowing a flap of face sheet to open near the end of the ballistic event.

To better understand what had occurred within the sample, we collected x-ray computed tomograms (XCT) for the sample video imaged above, and several slices are shown in Fig. 11. Fig. 11(a) shows a cross-sectional slice through the center of the sample containing the directions transverse to extrusion. It reveals that the rear face sheet was loaded by a fracture conoid whose dorsal width was about two unit cells wide (56 mm) and had an unusually acute conoid angle of 30° controlled by the web inclination angle. The heavily microcracked material within the fracture conoid loaded the rear face sheet, and the vertical cracks seen in Fig. 10 propagated by tearing (in the panel extrusion direction) of a pair of face sheet-web nodes bounding the conoid.

Fig. 11(b) shows a planar slice through the sample just beneath the impacted face sheet. It is aligned with the cross-sectional view above. The bases of the ceramic prisms (light grey) and the corrugated trusses (darker grey) can be clearly seen. Circumferential and radial cracking of the ceramic is seen, together with a heavily comminuted region[3] near the impact site. It is notable that the comminuted region is oval in section rather than the circular section of fragmentation conoids seen in impacted monolithic ceramic plates [19]. Fig. 11(c) and (d) corresponds to regions at the mid-plane and just above the rear face sheet of the sample. The discontinuous pattern of radial and circumferential cracks extended from the

[3] A region of multiply fractured ceramic.

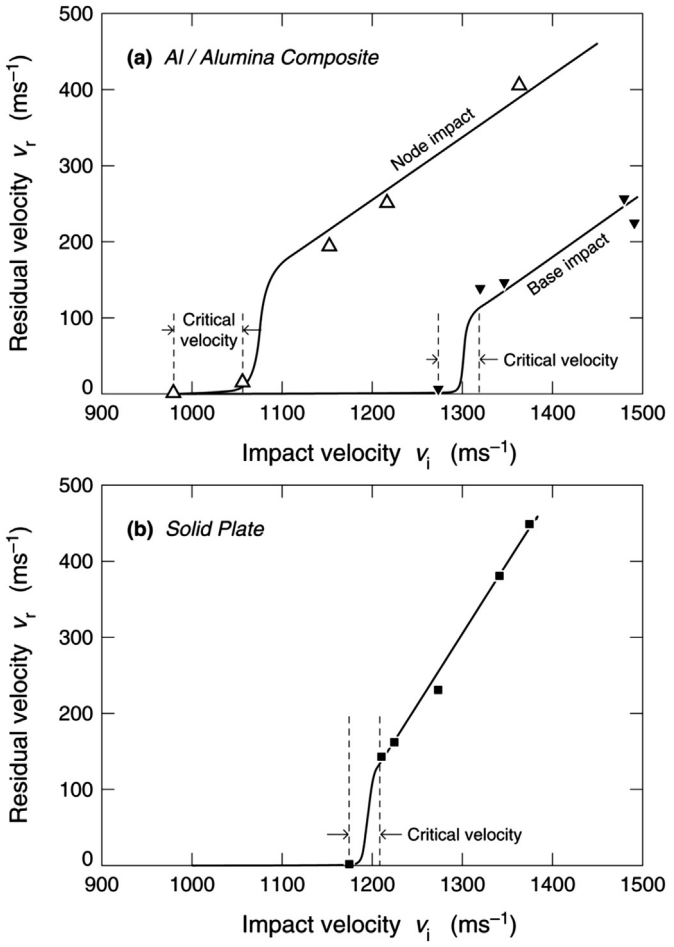

Fig. 9. (a) Residual velocity (component perpendicular to back face) versus impact velocity for the Al/Al_2O_3 composite sandwich panel impacted at either a node or prism base. The areal density of the panel was 97 kg m^{-2}. (b) Ballistic resistance curve for a solid aluminum plate of similar aerial density (98.9 kg m^{-2}) to composite panels.

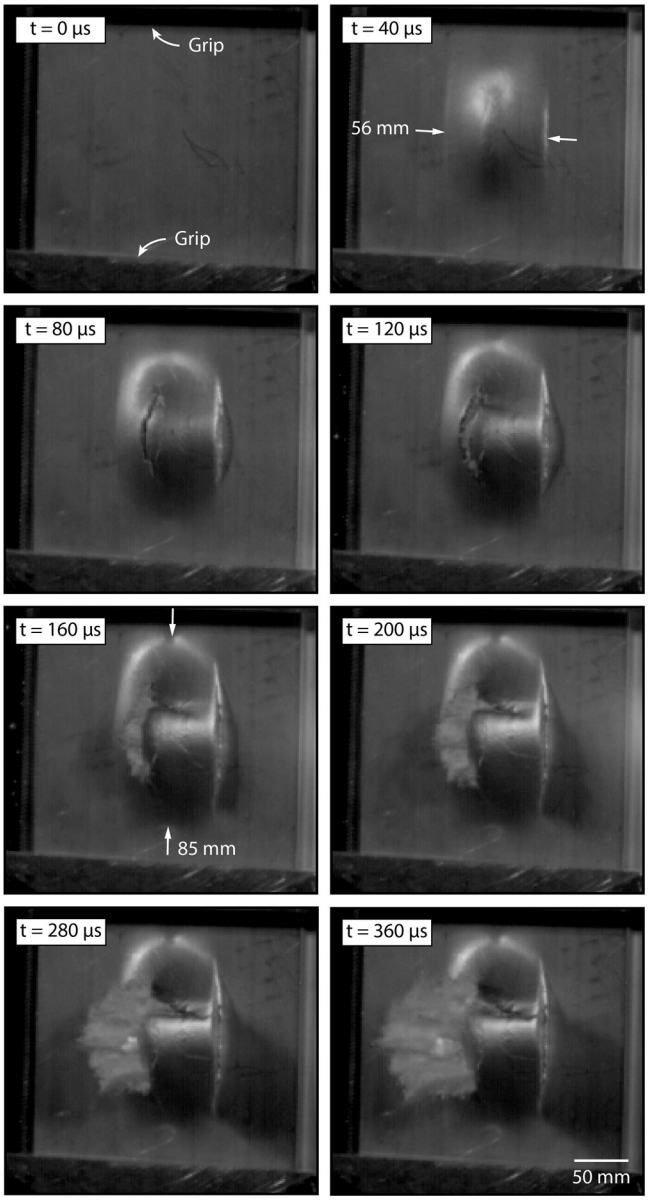

Fig. 10. High-speed image sequence of the back of a panel impacted at a prism base at a velocity of 1492 m s^{-1}.

impact site though the impacted ceramic prism and into one prism on either side. An oval cross section fracture conoid was again observed, and the conoid width in the extrusion direction grew with depth. The width of the conoid transverse to the extrusion direction is clearly bounded by the outermost webs of the prisms on either side of the one directly impacted. Lateral deflection, stretching and fracture of the trusses bounding the impacted prism are seen in these tomograms.

Fig. 11(e) shows a slice through the center of the target showing a plane containing the extrusion direction (at 90° to that of Fig. 11(a)). It can be seen the length of the deformed back face in the direction of extrusion was about 92 mm; very similar to that seen in the high-speed video images (Fig. 10). The comminuted ceramic within the conoid section viewed in this plane had a similar angle (60–65°) to that normally seen in impacted ceramics, and extended in length about the same distance as the back face sheet deformation. Less connected cracks in the ceramic are visible and some extended to the ends the ceramic prism.

The impacted samples were sectioned and the effect of increasing the impact velocity for a base impact is shown in Fig. 12. At low velocities, the projectile impacted a ceramic supported front face sheet. The photograph, Fig. 12(a), shows significant thickening of the aluminum face sheet and no plug between the project and the ceramic. This face sheet was penetrated by a ductile hole enlargement mechanism. The projectile underwent severe plastic deformation and shear fracture upon impact with the base of the ceramic prism. Significant comminution of the ceramic occurred under the projectile and long, shallow angle cone cracks had formed in the impacted prism and those on either side of it. A close up of the comminuted region and deformed/fractured projectile is shown in Fig. 13. The impact surface of the projectile has been flattened against the ceramic and there is severe cracking of the projectile that extends to its opposite side. The depth of penetration into the ceramic was 3 mm for an impact velocity of 656 m s^{-1}.

As the impact velocity increased, the projectile was fully defeated; small pieces of the projectile can be seen on the impact surface of the ceramic, Fig. 12(b). We therefore conclude that the projectile was arrested by interface defeat. The front face sheet impact crater grew in diameter, and suffered increasingly larger out of plane deflections with impact velocity increase. This out of plane motion, in the opposite direction to that of the projectile, was eventually sufficient to cause rupture of nodal connections between the face sheet and the core, Fig. 12(d) and (e). Increasing the

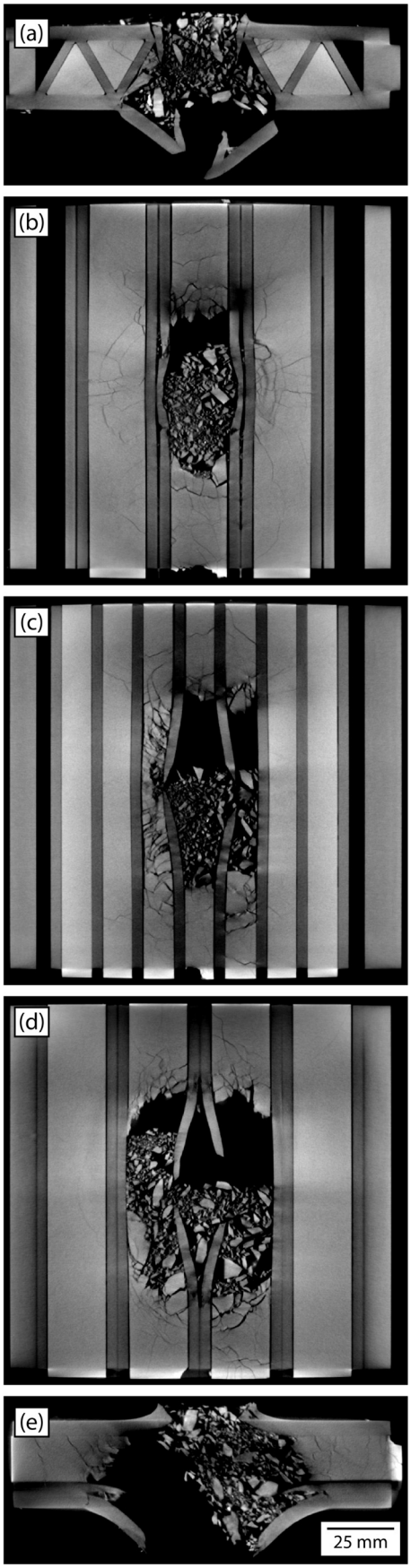

Fig. 11. XCT cross-sectional views of a base impacted panel. The projectile's impact velocity was 1492 m s^{-1}.

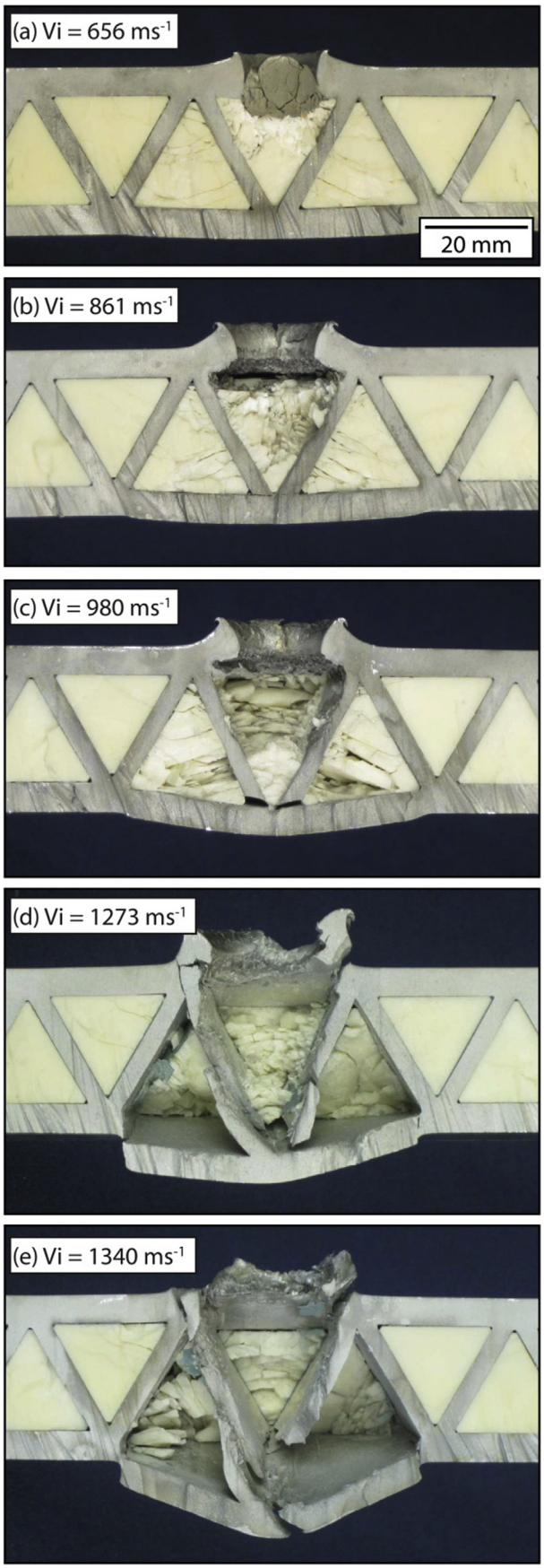

Fig. 12. Cross-sections of prism base impacted panels.

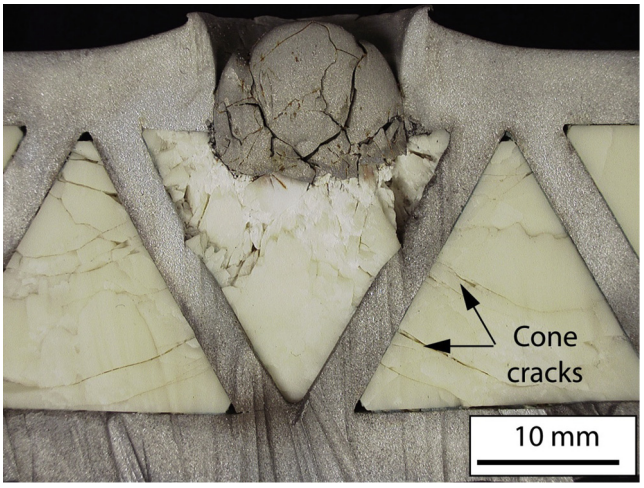

Fig. 13. Micrograph showing damage to projectile and panel after base impact at 656 m s^{-1}.

impact velocity also increased the volume of comminuted ceramic, but had little effect upon the lengths or inclination of the cone cracks which were confined to the impacted prism, and those on either side of it, Fig. 12(c)–(e).

As the impact velocity approached 980 m s^{-1}, the back face sheet began to bend and stretch, leading to tensile failure at the web-face sheet node directly beneath the impact location, Fig. 12(c). Photographs of the rear face of the samples, Fig. 14(a)–(c), shows that the length of these cracks in the extrusion direction grew with increase in impact velocity. Erosion of the webs and some tensile fractures were also seen, Fig. 12(d). Fracture of the back face sheet occurred by shear failure at a web supported node, and was initiated at impact velocities of about 1270 m s^{-1}, Fig. 12(d). Full penetration of the targets, Fig. 12(e), was facilitated by dorsal face sheet fracture over a two unit cell wide strip that extended in the longitudinal direction a distance of 82 mm for impact at 1219 m s^{-1} and about 95 mm at 1270 m s^{-1}.

5.1.2. Nodal impacts

The back face deformation sequence for a target impacted at a node is shown in Fig. 15 for an impact velocity of 1063 m s^{-1} – just slightly above the critical velocity. A rectangular strip of the back face was again outwardly displaced. Its width was a half that of the base impact while the length in the vertical (extrusion) direction reached 58 mm (just over twice the crack pair separation width). A small quantity of powdered material was again ejected at a shallow angle to the back face surface normal.

This target was examined with XCT to investigate the internal damage mechanisms, Fig. 16. The cross-sectional view, Fig. 16(a), shows that the projectile penetrated the front face with formation of a significant impact crater. Impact with the apex of the triangular cross section ceramic resulted in heavy comminution of the alumina, and the pushing of heavily damaged material within the fracture conoid against the dorsal face sheet causing substantial out of plane deformation, and shear failure at the truss-face sheet nodal locations. In the transverse plane, the fracture conoid that loaded the back face sheet was approximately one unit cell wide, and again had a very shallow conoid angle of 30° defined by the inclination angle of the webs. Some of the (white) debris from the projectile is piled-up at the (left) truss-face sheet node (the one that had opened sufficiently to allow a small quantity of ejecta to be emitted). The face sheet's out of plane deflection was also facilitated by fracture of one of the truss-face sheet nodes.

It is interesting to note that the aluminum trusses were effective at arresting cracks in the ceramic. However, they did stop the nucleation of new cracks in adjacent prisms. Fig. 16(b) shows a

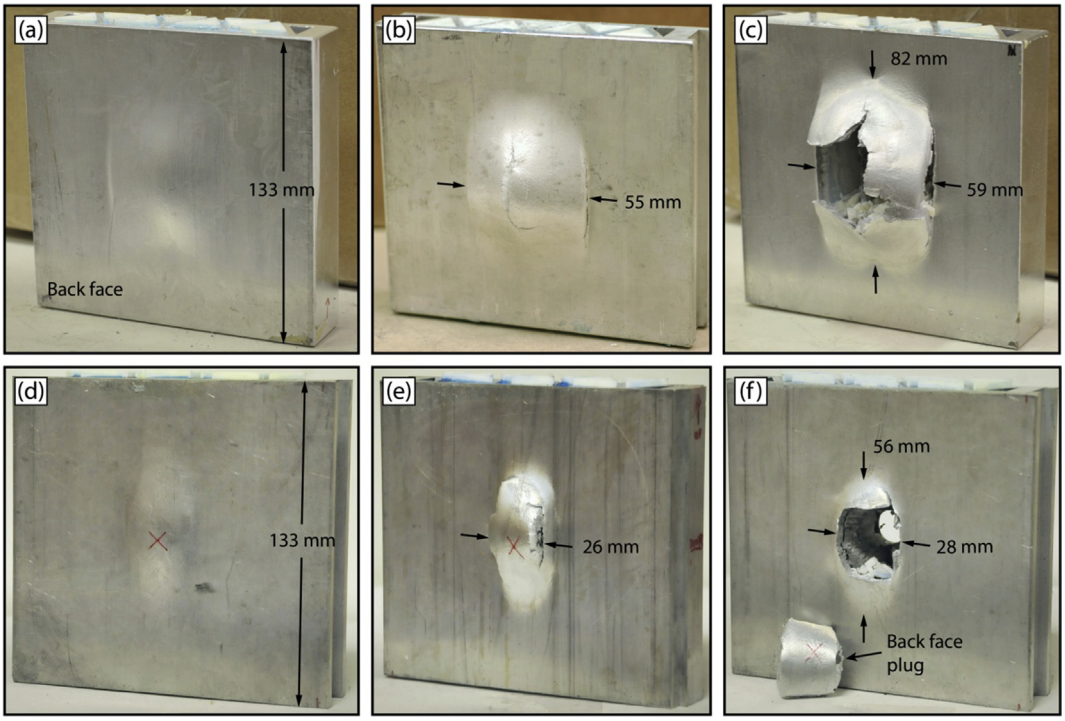

Fig. 14. Photographs of the back face of tested panels. Top row: Base impacts at velocities of (a) 980 m s^{-1}, (b) 1340 m s^{-1} and (c) 1606 m s^{-1}. Bottom row: node impacts at velocities of (d) 983 m s^{-1}, (e) 1154 m s^{-1} and (f) 1219 m s^{-1}.

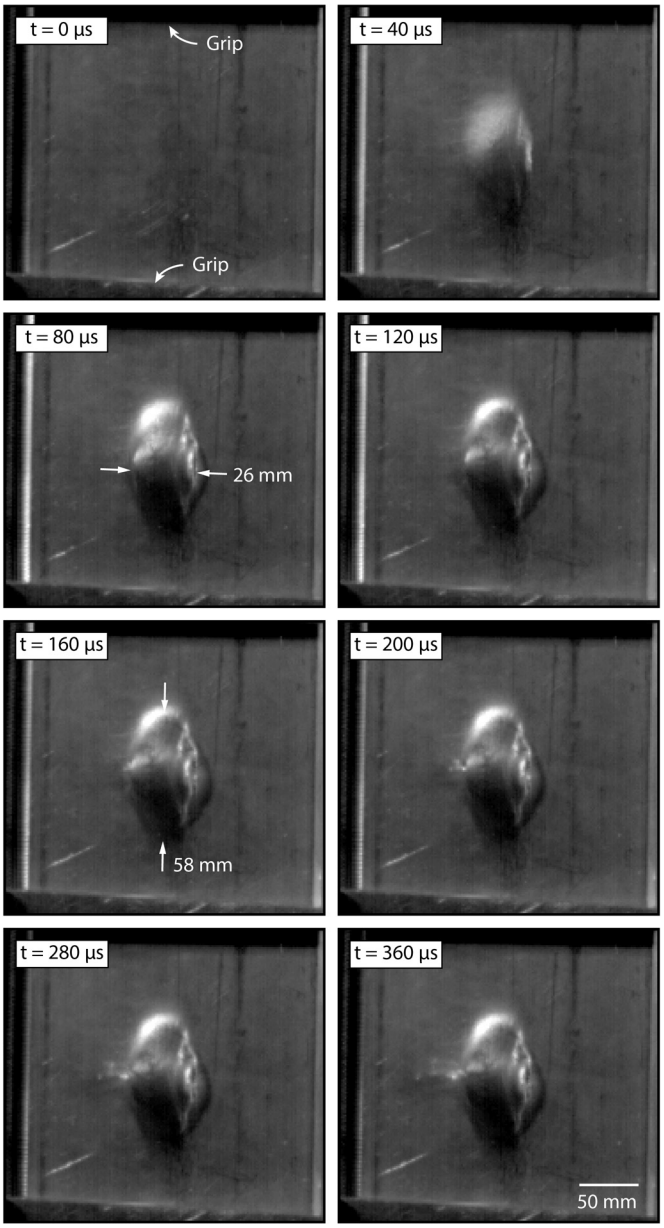

Fig. 15. High-speed video image sequence of the back surface of a test panel after nodal impact at a velocity of 1063 m s^{-1}. The corrugation (extrusion) direction was vertical.

planar view of the test structure just below the impacted front face sheet. The brighter grey material is the defeated projectile. Many fine cracks had formed in the bases of the two ceramic prisms located on either side of the prism whose apex was impacted. Some of the cracks extended almost the entire length of the prisms. Fig. 16(c) and (d) shows planar views at the mid-plane and bottom (dorsal) surface respectively of the ceramic filled core. Fig. 16(e) shows a longitudinal slice through the center of the impact and shows a more conventional conoid angle in the ceramic. The length of back face out of plane deflection in the longitudinal (extrusion) direction was governed by the footprint of the fracture conoid on the rear face sheet.

The evolution of target and projectile damage with increasing impact velocity is evident in Fig. 17. At low impact velocities, Fig. 17(a), the projectile readily penetrated the aluminum front face sheet forming a crater whose diameter increased with impact

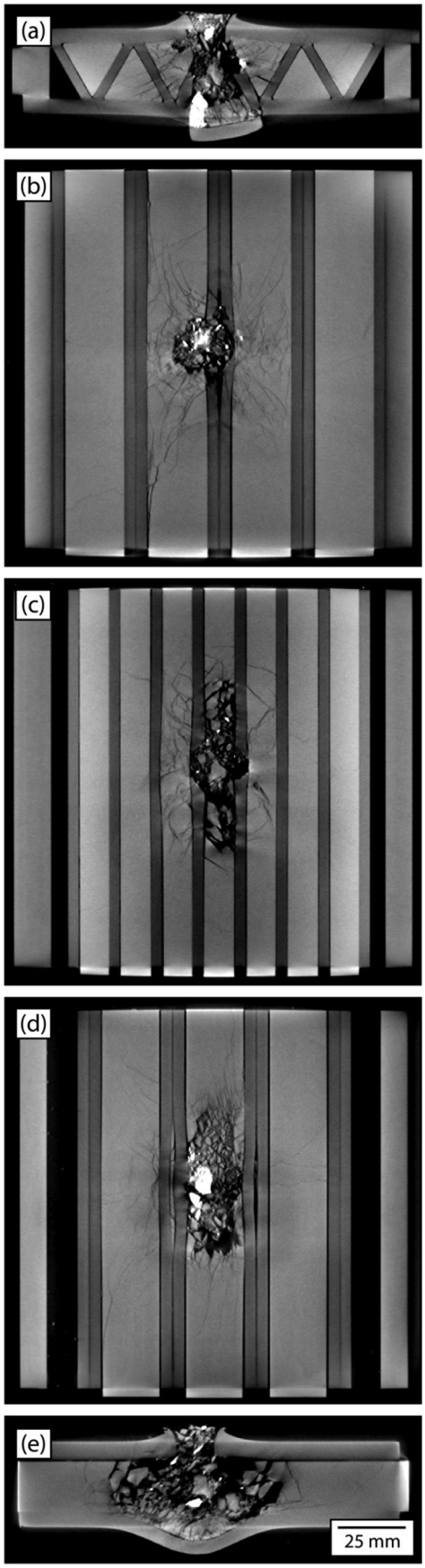

Fig. 16. XCT cross-sectional views of a panel impacted at a node at a velocity of 1063 m s^{-1}.

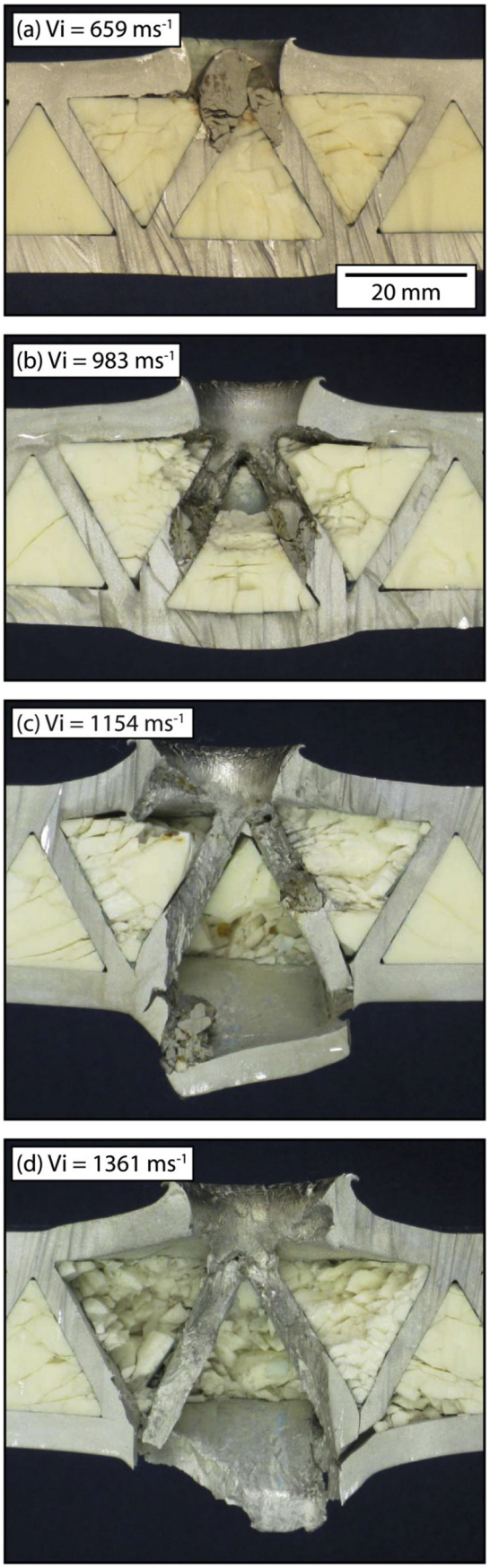

Fig. 17. Cross-sections of samples impacted at a node.

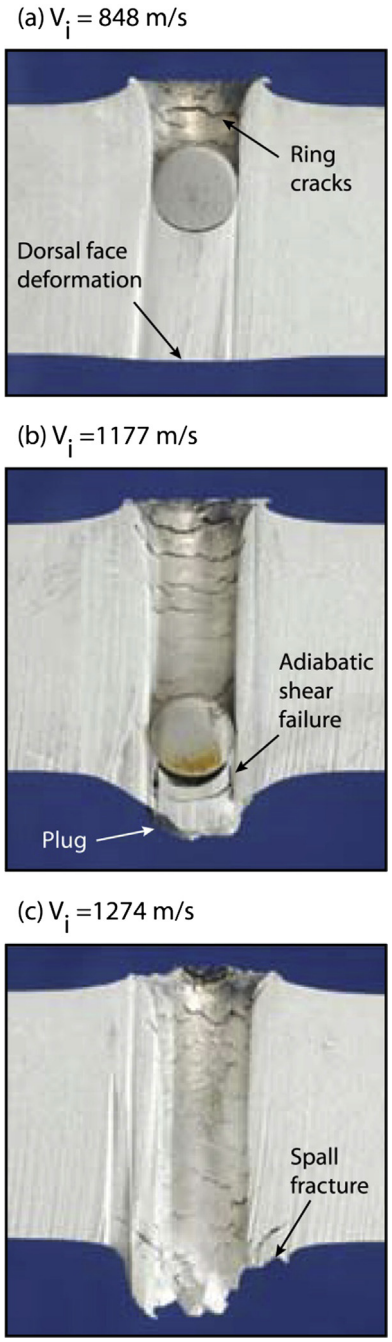

Fig. 18. Effect of increasing impact velocity on the penetration of 36.6 mm thick (aerial density of 98.9 kg m^{-2}) 6061T6 aluminum plates.

velocity. The projectile was severely deformed during its arrest against the apex of the aluminum web encased ceramic. The ceramic below the impact was less comminuted than for a comparable base impact, but the cone cracks extended through the impacted and adjacent prisms as before. The depth of ceramic penetration at an impact velocity of 659 m s^{-1} was 8.8 mm; about double that of a base impact. At higher velocities, Fig. 17(b), the projectile was fully defeated, but the depth of ceramic penetration had increased. The back face sheet between the nodes closest to the impact site also began to deform and bend out of the plane of the panel. Fracture of the dorsal face sheet was initiated at the prism – rear face sheet nodes resulting in a one prism base wide strip of dorsal face sheet undergoing failure in the extrusion direction, and

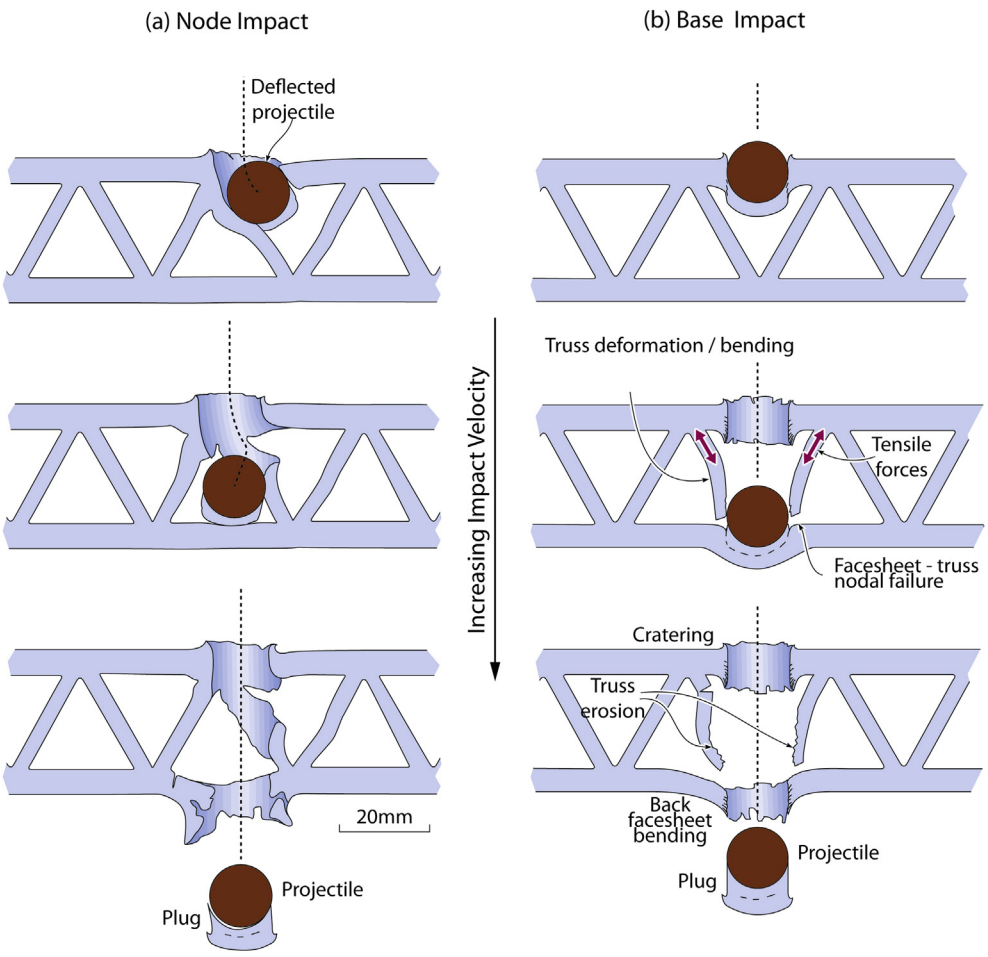

Fig. 19. Schematic illustration showing the effect of increasing the impact velocity on the damage mechanisms of the empty corrugated sandwich panels impacted at either (a) a node or (b) the base.

enabling ejection of comminuted ceramic and projectile debris. Comparison with Fig. 14 enables the effect of a base and nodal impact upon rear face deformation to be ascertained.

5.2. Equivalent solid plate response

Fig. 9(b) shows the residual verses impact velocity relation for a 36.6 mm thick Al6061T6 plate with a similar mass per unit area (98.9 kg m^{-2}) to the hybrid, ceramic filled panel. The critical velocity of this equivalent solid plate was approximately 1200 m s^{-1}; about 100 m s^{-1} above that of the hybrid panel impacted on at a node (ceramic prism apex) and about 100 m s^{-1} below that of a hybrid panel impacted on a ceramic base. Above the critical velocity, the residual verses impact velocity relation was linear with a slope of 1.85. This significantly exceeded the normal component of the residual velocity versus impact velocity slope (0.8) of the hybrid panels even when account is taken of the approximately 60° angle of ejecta emission.

Photographs of the penetrated region of water-jet sectioned samples impacted at 848, 1177 and 1274 m s^{-1} are shown in Fig. 18. It can be seen that the projectile suffered very little damage during the penetration process. At low impact velocity, Fig. 18(a) the projectile was arrested within the target after penetrating a distance that increased with impact velocity. Penetration occurred by ductile hole enlargement with a crater forming at the impact site. A set of approximately equally spaced ring cracks had formed near the periphery of the cylindrical hole made by the projectile. Just below the critical velocity, Fig. 18(b), significant bulging of the distal face of the sample occurred, and a small plug bounded by adiabatic shear bands was evident. The exit process appears to have caused significant strain in material adjacent to the distal exit hole resulting in ring cracking on a plane inclined to the surface.

6. Discussion

Sandwich panel structures with triangular prismatic core structures have been fabricated from 6061 aluminum using an extrusion process that results in core-face sheet nodal connections with a strength and ductility similar to those of the parent alloy. They have attracted interest as multifunctional structures capable of efficient structural load support while also mitigating shock loading effects [15]. The experimental study conducted here indicates that redistributing the mass of a (15.9 mm thick) solid 6061T6 aluminum alloy plate into the form of a corrugated core sandwich panel significantly changes the mode of non-deforming, spherical projectile penetration from adiabatic shear band facilitated shear-off with plug formation, to plugging of the front and rear faces of the sandwich with tensile stretching of core webs.

The study has also revealed that the penetration mechanism of the sandwich structures by projectiles, whose diameter was about one half the cores cell size width, depended upon the proximity of the impact site to a web-face sheet node. The panel's response to impacts at the nodal and base locations is compared schematically

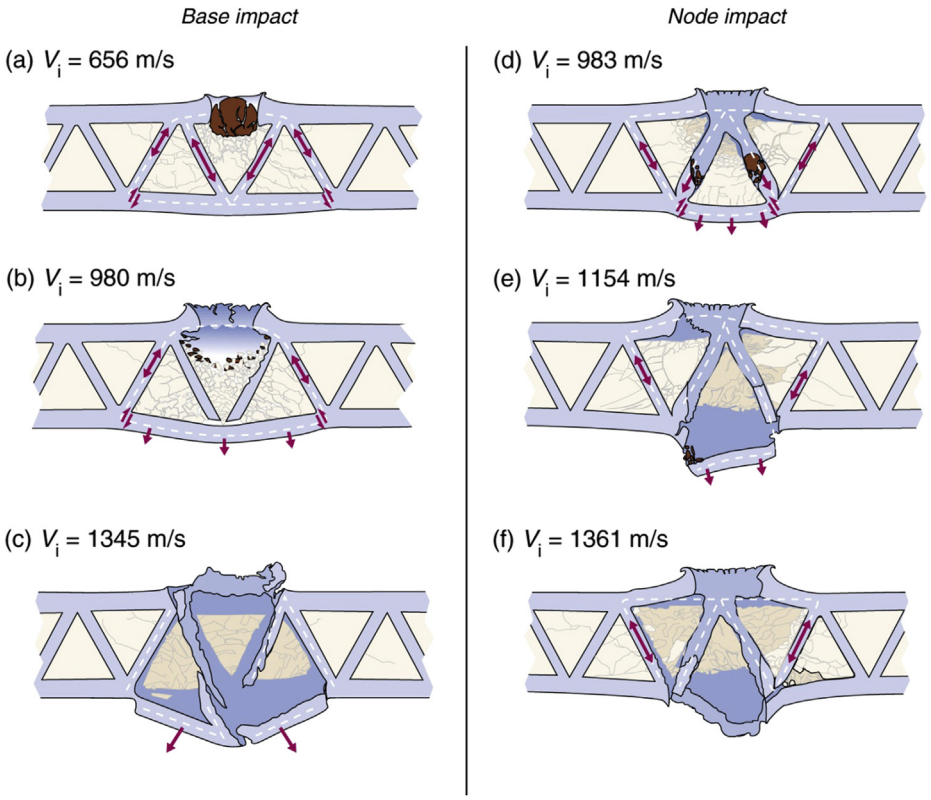

Fig. 20. Schematic showing damage mechanisms of panels impacted at the base at velocities of (a) 656 m s^{-1}, (b) 980 m s^{-1} and (c) 1345 m s^{-1}, and at a node at velocities of (d) 983 m s^{-1}, (e) 1154 m s^{-1} and (f) 1361 m s^{-1}.

in Fig. 19. Sub critical velocity projectiles that impact near a node can be significantly deflected by the webs. However, as the projectile momentum increases, the forces activated by impact with the webs become insufficient to deflect the projectile, and core penetration switches to web plate plugging. In contrast, impacts mid-way between pairs of nodes result in projectile impact with V-shaped webs on either side of the projectile. The lateral deflection forces exerted by each web approximately balance, and the projectile is not deflected. Projectile impact with the bottom half of the V-shaped region causes web stretching and fracture (in tension) at the web-dorsal face sheet nodal interface. In both cases the critical velocity is reached when the projectile penetrates the dorsal face sheet by plugging, and is independent of impact location for the sandwich design studied here.

Interestingly, the critical velocity for the sandwich panel with a core relative density of 25% was about 20% lower than that of the equivalent solid. Experiments with stainless steel sandwich panels that had much smaller (2.6%) core relative densities had ballistic limits only a few percent lower than the solid equivalent plate. These results indicate the thickness of the (face sheet) in which plug formation occurs control's penetration resistance [18]. In other words, the plastic work dissipated in the solid plate by radial flow, plug compression and adiabatic shear exceeds that of the less plastically confined (thin) face sheets and the stretching, bending and tensile fracture mode of the core webs of the sandwich.

These observations suggest that if the sandwich panel design were modified, the critical velocity might be made closer that of the equivalent solid plate. For example, if less mass were allocated to the front face sheet, and instead used to create thicker core webs, much more lateral deflection of projectile impacts near nodes might be achieved and the onset of web penetration delayed sufficiently to increase the critical velocity. The use of alternative materials with higher ductility, or work hardening or strain rate strengthening might also result in a different response. An efficient investigation of these effects awaits the emergence of computational tools that can reliably predict large plastic strain trajectories and fracture paths.

Filling the core of a sandwich structure with ballistic grade alumina prisms profoundly changes the mechanisms of penetration. The projectile is heavily deformed and fractured well before the ballistic limit is reached. The mechanisms of penetration at the ballistic limit are again dependent upon the location of impact. At low projectile speeds, impacts at the base of a ceramic prism result in front face sheet penetration by ductile hole expansion followed by severe plastic deformation of the projectile at the ceramic surface, Fig. 12(a) and 13. Radial and circumferential cracks are observed in the impacted prism and in those next to it. However we note that the cracks in adjacent prisms are not extensions of those in the primary prism; these are invariably arrested by the metallic core webs.

As the impact speed increases, fragmentation of the projectile occurs at the primary ceramic prism front face and is accompanied by significant comminution of the ceramic and formation of an oval cross section fracture conoid. This conoid loads the rear face sheet, causing it to undergo deflection and stretching, Fig. 12(c). Penetration at the critical velocity occurs when a rectangular region of the distal face suffers fracture along a pair of core web-face sheet nodes, Fig. 12(d). For a base impact approaching the ballistic limit, the fracture conoid angle in the transverse plane is acute and controlled by the web inclination. When material within the displaced conoid loads the distal face sheet, a pair of longitudinal fractures, with a two cell width separation, is formed. While the width of the distal separation distance remains fixed, the crack lengths in the extrusion direction increase with impact velocity, as does the area of the out of

plane deformed/fractured sheet. Small increase in impact velocity lead to a third collinear crack mid-way between the first two, Figs. 12(e) and 11(a). The progressive activation of this sequence of failure mechanisms as the impact velocity increases is schematically illustrated in Fig. 20(a–c).

Nodal impacts at a ceramic prism apex also lead to projectile deformation and break-up as the impact speed increases. Careful examination of Fig. 17(a) shows that the projectile deforms around the apex of the ceramic prism and begins to flow along the aluminum webs. This is accompanied by ceramic comminution in the impacted and adjacent prisms, and a rigid body displacement of the apex impacted (microcracked) prism in the impact direction. This results in a displacement of the face sheet in contact with the base of the prism, and the eventual formation of longitudinal cracks at the web/face sheet interfaces. This pair of cracks then allows the distal face sheet to peel and ejecta to be emitted from the rear of the target. These phenomena are similar to those seen for impacts of a prism base, but the distal face sheet crack separation (and thus width of the region through which debris is ejected from the rear of the target) is only a half that of the former case. The mechanisms induced by the two impact scenarios are schematically compared in Fig. 20(d–f). They demonstrate that cellular structures provide novel opportunities to control the fracture conoid angle, and thus the shape and dimensions of the load footprint applied to the rear face sheet.

Impacts with a prism base were more effective at retarding projectile penetration and had a critical velocity ~ 200 m s^{-1} higher than that of a nodal impact. Penetration of the equivalent solid aluminum plate at these impact velocities still occurred by a plugging mechanism and had a critical velocity ~ 100 m s^{-1} higher than a prism apex impact and only ~ 100 m s^{-1} less than that of a base strike. The spherical projectile penetration mechanisms identified above indicate promising avenues for explorations of structures with higher critical velocities. For example, since the critical velocity is associated with rupture of the distal face sheet, reallocation of aluminum mass to this face appears a promising strategy for improving impact resistance. The use of higher strength alloys for the encasement and harder ceramics would also be promising avenues of further investigation. We note that the ceramics were not highly confined in these targets and that this can substantially increase ballistic resistance [20]. Recent micromechanics based studies indicate that hard materials with higher crack growth resistances and more acute fracture conoid angles, such as nickel bonded TiC (cermets), might also be well suited for manipulating the support plate loading footprint [21].

7. Conclusions

An experimental study of the penetration mechanisms of 6061T6 aluminum extruded, corrugated core sandwich panels has been conducted and contrasted with those of equivalent solid aluminum plates of identical mass per unit area. The response of both empty core and alumina filled structures has been investigated using a model 12.7 mm diameter spherical projectile made of high strength steel. The diameter of the projectile was about a half the base width of the triangular cross section corrugations. We find that:

1. The mechanisms of penetration of the empty sandwich structure involve plug formation in the impact and distal face sheets and stretching, bending and fracture of the core webs. For the structures investigated here, these mechanisms were less effective at impeding projectile penetration than a solid equivalent plate penetrated by adiabatic shear.
2. The mechanism of interaction of the sandwich structure with the projectile depended upon the location of the impact with respect to the web/face sheet node. Low momentum impacts near a node penetrated the impact face sheet but were then laterally deflected by the inclined web, raising interesting opportunities to manipulate the ballistic response by allocating more of the extrusion mass to the core at the expense of the front face thickness.
3. Filling the triangular spaces within the corrugated core with ballistic grade alumina prisms led to severe projectile plastic deformation and fragmentation as the impact speed was increased. Penetration was then controlled by the shape of the oval fracture conoid which loaded, and fractured the distal face sheet. The conoid section aspect ratio depended upon the location of the impact with respect to that of the web/face sheet nodes. Impacts near a node at the critical velocity resulted in pairs of distal face fractures separated by one cell running a much longer distance in the original extrusion direction. For impacts on the base of a prism (mid-way between pairs of nodes), the transverse cracks were twice as widely separated as those of a nodal impact.
4. The half angle of the webs of the corrugated core defined the fracture conoid angle on the transverse plane. This creates interesting possibilities for improving the ballistic response to a second, nearby impact in this direction.
5. For the structures explored here, the penetration resistance of the ceramic filled structures was about 100 m s^{-1} higher than the equivalent solid plate for base impacts, and about 100 m s^{-1} less than the solid plate when impacts struck a node. The mechanisms of penetration suggest that reallocating extrusion mass from the impacted to distal face sheet may improve the ballistic resistance of the structure.

Acknowledgements

We are grateful to B.G. Compton, E.A. Gambell and F.W. Zok at UCSB for their assistance with some of the ballistic testing. The project was funded by the Office of Naval Research (ONR) under grant number N00014-07-1-0764 (Program manager, Dr. D. Shifler) and the Defense Advanced Research Projects under grant W91CRB-11-1-0005 (Program manager, Dr. J. Goldwasser).

References

[1] (Gama) Haque BZ, Harrington JL, Gillespie Jr JW. Multi-hit ballistic impact on S-2 glass/SC15 thick-section composites: experiments. The Journal of Strain Analysis for Engineering Design 2012;47:480–94.
[2] Anderson Jr CE, Rotal-Timmons SA. Ballistic performance of confined 99.5%-$A1_20_3$ ceramic tiles. International Journal of Impact Engineering 1997;19:703–13.
[3] Fink BK. Performance metrics for composite integral armor. Journal of Thermoplastic Composite Materials 2000;13:417–31.
[4] Evans AG, Hutchinson JW, Ashby MF. Multifunctionality of cellular metal systems. Progress in Materials Science 1999;43:171–221.
[5] Dharmasena KP, Wadley HNG, Xue Z, Hutchinson JW. Mechanical response of metallic honeycomb sandwich panel structures to high intensity dynamic loading. International Journal of Impact Engineering 2008;35:1063–74.
[6] Hutchinson JW, Xue Z. Metal sandwich plates optimized for pressure impulses. International Journal of Mechanical Sciences 2005;47:545–69.
[7] Deshpande VS, Fleck NA, Ashby MF. Journal of the Mechanics and Physics of Solids 2001;49:1747–69.
[8] Pingle SM, Fleck NA, Deshpande VS, Wadley HNG. Collapse mechanism maps for a hollow pyramidal lattice. Proceedings of The Royal Society A 2011;47:985–1011.
[9] Deshpande VS, Fleck NA. One-dimensional response of sandwich plates to underwater shock loading. Journal of the Mechanics and Physics of Solids 2005;53:2347–83.
[10] Wicks N, Hutchinson JW. Optimal truss plates. International Journal of Solids and Structures 2001;38:5165–83.
[11] Liang Y, Spuskanyuk AV, Flores SE, Hayhurst DR, Hutchinson JW, McMeeking RM, et-al. The response of metallic sandwich panels to water blast. Journal of Applied Mechanics 2007;74:81–99.

[12] Hutchinson JW. Energy and momentum transfer in air shocks. Journal of Applied Mechanics 2009;76:051307-1–051307-7.
[13] Tang Xin, Prakash Vikas, Lewandowski John J, Kooistra Gregory W, Wadley Haydn NG. Inertial stabilization of buckling at high rates of loading and low test temperatures: implications for dynamic crush resistance of aluminum-alloy-based sandwich plates with lattice core. Acta Materialia 2007;55:2829–40.
[14] Russell BP, Malcom AJ, Wadley HNG, Deshpande VS. Dynamic compressive response of composite corrugated cores. Journal of Mechanics of Materials and Structures 2010;5:477–93.
[15] Rimoli JJ, Talamini B, Wetzel JJ, Dharmasena KP, Radovitzky R, Wadley HNG. Wet-sand impulse loading of metallic plates and corrugated core sandwich panels. International Journal of Impact Engineering 2011;38:837–48.
[16] Kambouchev N, Noels L, Radovitzky R. Fluid–structure interaction effects in the loading of free-standing plates by uniform shocks. Journal of Applied Mechanics 2007;74:1042–5.
[17] Wei Z, Deshpande VS, Evans AG, Dharmasena KP, Queheillalt DT, Wadley HNG, et-al. The resistance of metallic plates to localized impulse. Journal of Mechanics and Physics of Solids 2008;56:2074–91.
[18] Yungwirth Christian J, O'Connor John, Zakraysek Alan, Deshpande Vikram S, Wadley Haydn NG. Explorations of hybrid sandwich panel concepts for projectile impact mitigation. Journal of the American Ceramic Society 2011;94:S62–75.
[19] Woodward RL. A simple one-dimensional approach to modeling ceramic composite armour defeat. International Journal of Impact Engineering 1990;9:455–74.
[20] Compton BG, Gamble EA, Deshpande VS, Zok FW. Damage development in an armor alumina impacted with ductile metal spheres. Journal of Mechanics of Materials and Structures 2012;7:575–91.
[21] Compton BG, Zok FW. Impact resistance of TiC-based cermets. International Journal of Impact Engineering 2013;62:75–87.